Enhanced high performance of aluminum/indium Co-doped lithium nickel manganese cobalt oxide for possible batteries application

S. R. Kadum[a], A. S. Baron[b], H. M. J. Haider[a*]
[a]*Department of Physics, Faculty of Education for Girls, University of Kufa, Kufa, Iraq*
[b]*Department of Physics, Faculty of Science, University of Kufa, Kufa, Iraq*

In this study, the $Li[Li_{0.20}Ni_{0.13}Co_{0.13-y}Mn_{0.54-x}]Al_yIn_xO_2$ was synthesized via sol-gel method. electrochemical and structural attributes of nanopowders determined by the thermal analysis (TGA)/(DTA), structural analysis (XRD), (FESEM), chemical analysis (EDS) and (FTIR), BET analysis and their results appraised. X-ray diffraction analysis were performed to study the formation of nanopowders, illustrating the α- $NaFeO_2$ structure with $R\bar{3}m$ space group. FESEM Figures showed that the nanopowders have a group of the cubic and the hexagonal particles. Chemical test of the EDS proved the existence of Aluminum and Indium. TGA/DTA tests for the displayed weight loss in the nanopowders. Infrared spectroscopy studied connectivity bonds and chemical elements that are utilized in the cathode. The powders with Al (y = 0.02) and In (x = 0. 01) represented the high cycling efficiency and have better discharge capacity. $Li[Li_{0.20}Ni_{0.13}Co_{0.13-0.02}Mn_{0.54-0.01}]Al_{0.02}In_{0.01}O_2$ displayed the higher cycling consistency and the better capacity in collation with those of the non-replacement powders. Electrochemical impedance spectroscopy (EIS) showed that adding the Indium-Aluminum impurities improved the electrochemical efficiency of the $Li[Li_{0.20}Ni_{0.13}Co_{0.13}Mn_{0.54}]O_2$.

(Received August 13, 2023; November 30, 2023)

Keywords: The $Li[Li_{0.20}Ni_{0.13}Co_{0.13}Mn_{0.54}]O_2$, sol-gel, In-Al co- embedment, The structural consistency, The discharge-Capacity

1. Introduction

Decreasing the fossil fuel utilization by expanding efficient batteries for storing electrical energy is necessary to attain the supportable transport system, and also to meet the growing need of mankind for clean and safe energy [1].

Between the different Li-ion batteries, Mn-based lithium-rich cathode substances have attracted much consideration due to their high capacity and decreased toxicity and cost [2]. Although, reversibility of capacity in the first cycle is a major disadvantage that limiting their applicability. This is dependent on derivation of the lithium in the shape of Li_2O when the charging of the battery is done at more than 4.5 V that is referred to as lithium removal procedure [3]. The initial disinsertion process may be due to the removal of the oxygen vacancies from lattice that reduces the number of insertion/ disinsertion lithium ion sites in the discharge process [4]. Most recently, many endeavors have been made to dominate the difficulties and enhance the electrochemical performance of Mn based Li-rich cathode substances, such as doped with various elements [5-11]. Dorn et al. [12] reported that Al doping improves reversibility and increases electron conductivity. Doping with one of the metal elements alone is not able to protect the electrode surface from degradation and accumulation of inactive species resulting from electrolyte decomposition or the reaction of the electrode and electrolyte [13-19]. Therefore, we need to look for a new combination of two elements doping same time with tow element to take advantage of the effective of both. In this research, Indium and Aluminum elements are utilized as the succession and their impact on the structural, morphological and the electrochemical efficiency of doped - undoped nanopowders are studied.

* Corresponding authors: hayderm.alhayderi@uokufa.edu.iq
https://doi.org/10.15251/DJNB.2023.184.1493

2. Experimental

2.1. Preparation of materials

The sol-gel procedure is used to synthesize of the $[Li_{0.20}Ni_{0.13}Co_{0.13}Mn_{0.54}]O_2$ (NCM). Firstly, a transparent hydrous solution comprising the nitrates of the metal and the citric acid was provided in a stoichiometric amount. The oxidizing stoichiometric ratio was adjusted for the unit diminishing agent to ensure that maximum heat is abandoned. The humid gel was located in a vacuum oven in 120°C for 12h, in order to delete the remnants and other organic materials from prepared gel. The eventuating gel pioneer is disjointed at the temperature of 500°C for 5 h in air. The heating process of disjointed powders is lasted for 6 h at the temperature of 850 °C. The quenching of the pellet in air at environment temperature is led to obtain final powders. The $Li[Li_{0.20}Mn_{0.54-x}Ni_{0.13}Co_{0.13-y}]In_xAl_yO_2$ material was combined in the same way as before, but by simultaneously adding another necessary value, in $Al(NO_3)_3.9H_2O$ and $InCl_3$ in the amounts stoichiometric.

TGA/DTA tests were used for the doped and undoped nanopowders to characterize the crystal structure of the powders of as-accumulated $Li(Li_{0.20}Mn_{0.54}Ni_{0.13}Co_{0.13})O_2$ and $Li[Li_{0.20}Mn_{0.54-x}Ni_{0.13}Co_{0.13-y}]In_xAl_yO_2$ with STA PT 1600 TG-DTA device (LINSEIS) in air. (The characterizing of lattice structure of the powders of as-synthesized $Li(Li_{0.20}Mn_{0.54}Ni_{0.13}Co_{0.13})O_2$ and $Li[Li_{0.20}Mn_{0.54-x}Ni_{0.13}Co_{0.13-y}]In_xAl_yO_2$ was carried out by TGA/DTA tests for the doped and undoped nanopowders with STA PT 1600 TG-DTA device (LINSEIS) at the heating rate of 10°C/min in air.). X-ray diffraction analysis was done by Bruker YT diffractometer using the CuKα radiation in 2θ domain of 10° to 80°. Size and morphology of this nanopowders are examined by the FESEM carry out on MIRA3TESCAN microscope equipped with EDX test. Infrared spectrum was recorded by AVATAR 370, Thermo Nicolet spectrophotometer.

2.2. Fabrication of Battery

2.2.1. Construction of Electrolyte

Construction of battery: To constructing electrolyte, the Li perchlorate salt is used without water and located in the vacuum oven for 24 h at 100 °C - 120 °C. When Li perchlorate is cooled, it is sent out and 1 M solution from it is collected in the $C_4H_6O_3$ solvent and utilized as electrolyte.

2.2.2. Procurement of the Cathodic Electrode:

To product, cathode electrode is used from Al foil of 200 microns thick as a flow gatherer and graphite is utilized to raise electrical conductivity of electrode. The cathode powder (85 wt%) and graphite (15 wt%) along with 5 wt% of Teflon PVDF emulsion diluted in NMP (to increase adhesion) were mixed together and deposited on Al foil. This electrode is dried-up in the vacuum oven at the temperature of 100 °C for at least 8 hours and finally, this cathode is compressed on the Al surface, in order to raise the constancy.

2.2.3. Describing the Battery Manufacturing:

A designed cell with two polymer plates is used to manufacture a battery, which inside of each of them comprises Al plates for the electrical junction with the electrodes. The anode electrode is in the form of a spherical plate with a suitable diameter, which is cut inside the glove box. A porous polypropylene polymer thin film called Selgard is used for the discriminator. To barricade the electrical connection, this discriminator is used, which is immersed in the electrolyte for 12 hours and is placed between the two electrodes. The cathode electrode is also placed in the same location on the inverse polymer plate. All these processes are carried out in a glove box under an argon atmosphere.

3. Results and Discussion

3.1. Thermogravimetric Investigation

TGA/DTA curves indicated in the Figure 1a and 1b are used for $Li(Li_{0.20}Mn_{0.54}Ni_{0.13}Co_{0.13})O_2$ and Indium-Aluminum co-doping in the $Li[Li_{0.20}Ni_{0.13}Co_{0.13}Mn_{0.54}]O_2$ nanopowders dry gel (Al=0.075% and In=0.02%) to consider the mass changes of the nanomaterials

in sol-gel procedure. In a undoped sample, feeble endothermic peak at about 280 °C in DTA plots of pure gel, that is consistent with the weight lesion equal to 15% in TG plot, is due to the elimination of the remaining water molecules. A weight loss (about 45%) is seen at 300 to 450°C, which is accompanied by a strong exothermic peak at 320°C. This weight loss is due to the decomposition and combustion of the clathrate, which is complete at 480°C.

In nanopowders having In-Al co-substitution, these peaks were nearly similar but the exothermic peak of about 200 °C has been observed, which attributed to decomposition of the hydroxyl group in the sample. The 2nd weight loss is likely because of formation of $Li(Li_{0.20}Mn_{0.54-x}Ni_{0.13}Co_{0.13-y})Al_yIn_xO_2$ crystal in 450-500°C Therefore, the pre-calcinations temperature of doped and undoped powders in the next experiment was selected at 500°C [20].

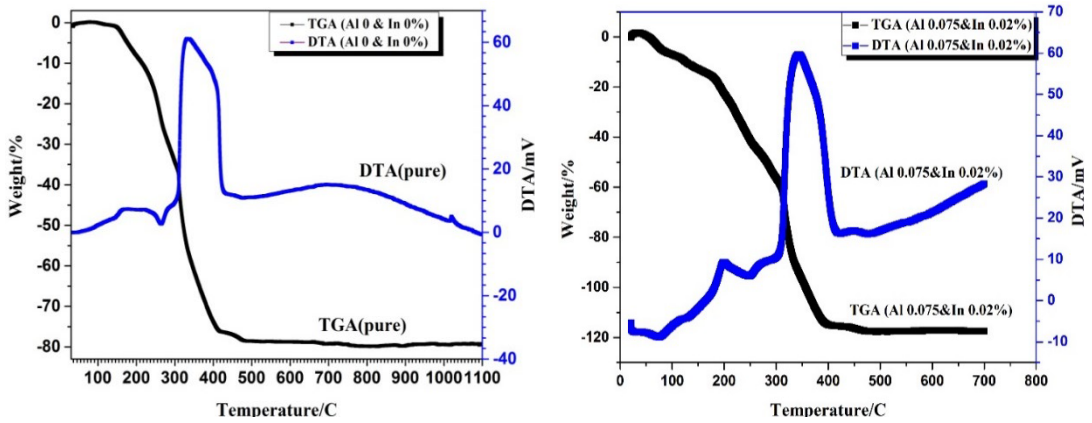

Fig.1 TGA/DTA curves for undoped $[Li_{1.20}Ni_{0.13}Co_{0.13}Mn_{0.54}]O_2$ and $[Li_{1.20}Mn_{0.54-x}Ni_{0.13}Co_{0.13-y}]Al_yIn_xO_2$ (y=0.075%, x=0.02%)

3.2. Structural properties

The XRD curves of the $Li[Li_{0.20}Ni_{0.13}Co_{0.13-y}Mn_{0.54-x}]O_2$ cathode powders consisting of various values of co-supersession doping Al-In (Al&In=0&0, 0.01&0.01, 0.02&0.01, 0.05&0.015, 0.075&0.02) are illustrated in Figure 2. This figure also shows that the co-supersession doping of Al-In with the additional amount of indium in x≥0.015, its structure was changed with impurity phase In_2O_3. Except for multiple weak peaks in the range of 20-25 °C, additional peaks in the figure 2 can be clarified as the α- $NaFeO_2$ layer structure with $R\bar{3}m$ space group. prior works have shown that these peaks are dependent to the ordering of the $LiMn_6$ cation [21].

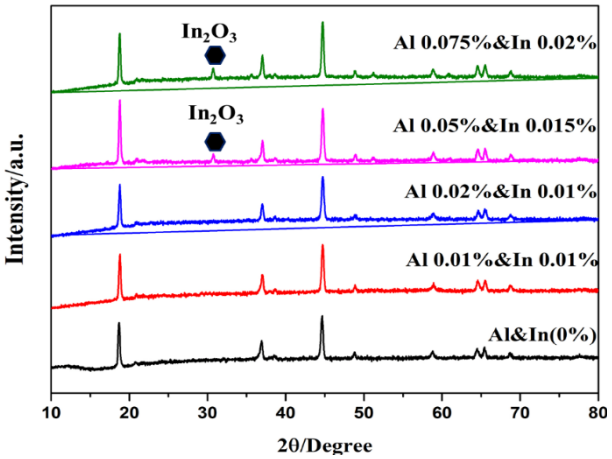

Fig. 2 The XRD patterns of undoped $[Li_{1.20}Ni_{0.13}Co_{0.13}Mn_{0.54}]O_2$ and $[Li_{1.20}Mn_{0.54-x}Ni_{0.13}Co_{0.13-y}]In_xAl_yO_2$ (x = 0, 0.01, 0.01, 0.015, 0.02%) and (y = 0, 0.01, 0.02, 0.05, 0.075%)

Fundamentally, the ratio of the peak intensity (003)/(104) is the scale of the dimensional cationic regularity [22] and when I(003)/I(104)<1.2, cation blending can inhibit lithiation and de-lithiation operation [23]. The higher values of c/a are attributed to the larger interior space of unit cell and simplify the widespread propagation route for the Li ions, which results in better electrochemical efficiency [24-25]. Unit cell parameters of the specimens were abbreviated in the Table 1.

Table 1. The Unit cell parameters of undoped $Li[Li_{0.20}Ni_{0.13}Co_{0.13}Mn_{0.54}]O_2$ and $Li[Li_{0.20}Mn_{0.54-x}Ni_{0.13}Co_{0.13-y}]In_xAl_yO_2$ (x = 0, 0.01&y=0.02).

Sample	a (A)	c (A)	c/a
$Li[Li_{0.20}Ni_{0.13}Co_{0.13}Mn_{0.54}]O_2$	4.928	9.604	1.948
$Li[Li_{0.20}Mn_{0.54-x}Ni_{0.13}Co_{0.13-y}]In_xAl_yO_2$	4.932	9.613	1.949

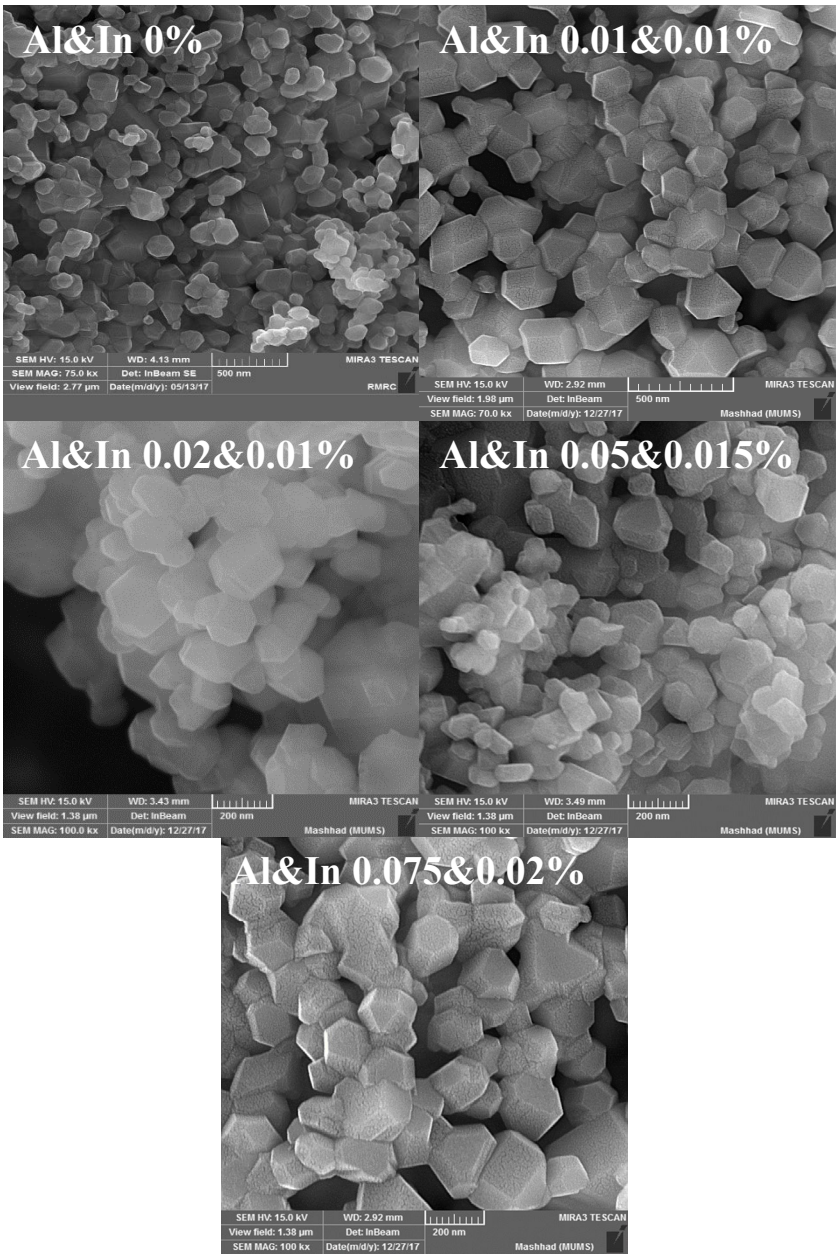

Fig. 3. FESEM photographs of undoped $Li[Li_{0.20}Ni_{0.13}Co_{0.13}Mn_{0.54}]O_2$ and $[Li_{1.20}Mn_{0.54-x}Ni_{0.13}Co_{0.13-y}]In_xAl_yO_2$ (x = 0, 0.01, 0.01, 0.015, 0.02%) and (y = 0, 0.01, 0.02, 0.05, 0.075%).

The lattice parameters a and c for undoped materials and doped In -Al materials comprising with different amounts of Indium and Aluminum were reported in the Table 1. It can be observed that with Indium-Aluminum co-doping in the $Li[Li_{0.20}Ni_{0.13}Co_{0.13}Mn_{0.54}]O_2$ cathode, the lattice parameters c, a and c/a increase, which leads to an enhancement in inter-slab spacing that simplifies the extraction and the insertion of Li^+ ions. Additionally, using the aluminum doping, the binding energy increases and leads to a significant decreasing due to the cation blending, which means that the Ni^{2+} and Li^+ ions exchange their collections in the layer structure. In addition, cycling efficiency can be better by reducing the cation blending [26].

The morphology of undoped and Indium-Aluminum co-substitution in the $Li[Li_{0.20}Ni_{0.13}Co_{0.13}Mn_{0.54}]O_2$ cathode is shown in Fig. 3. FESEM observations display which the particles have a monotonous particle size. Undoped materials have a larger number of agglomerated particles contrast to the doped material. moreover, the size of the bigger particles and the smoother morphology are perceived for the doped nano-material with the x and y amount of (Al&In=0&0, 0.01&0.01, 0.01&0.02, 0.015&0.05, 0.02&0.075).

It is observed that, the Powders morphology is directly related to electrochemical features of Li batteries. Therefore, powders having the hexagonal morphology and the homogeneous particle distribution exhibit a better electrochemical efficiency, such as the discharge capacity and the cycling efficiency [27].

Chemical composition of the nanopowders of Li $[Li_{0.20}Ni_{0.13}Co_{0.13-y}Mn_{0.54-x}]O_2$ (take x=0 and 0.01, y= 0 and 0.02% as an example) were analyzed by energy-dispersive X-ray analyzer (EDS) and are showed in Figure 4.

These figures show the sample EDS and emphasize that the Indium and Aluminum elements are distributed uniformly in the specimens.

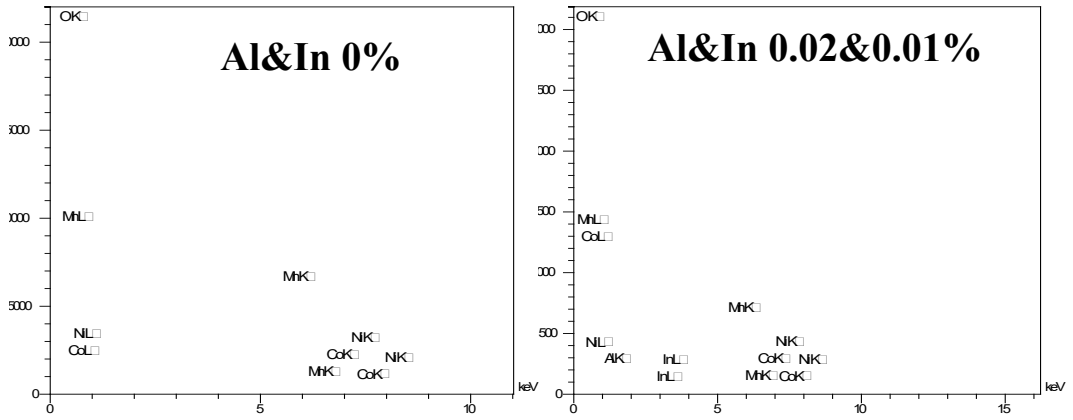

Fig. 4. The EDS patterns of the $[Li_{1.20}Mn_{0.54-x}Ni_{0.13}Co_{0.13-y}]In_xAl_yO_2$ (x = 0, 0.01% and y = 0, 0.02%).

The results of Fourier transform infrared spectroscopy for the undoped and the Indium-Aluminum co-substitution in $Li[Li_{0.20}Ni_{0.13}Co_{0.13}Mn_{0.54}]O_2$ nano-powders in the temperature of 500 °C and 850 °C between the wavelengths of 4000-500 Cm^{-1} showed in Figure 5. The peaks identified in the range of 500 to 700 Cm^{-1} are due to asymmetric stretching of Li-O bonds as well as M-O (M = Mn, Ni, Co) in MO_6. As observed in this Figure, for the undoped powders, a peak is detected in 3297.76 Cm^{-1}, which is attributed to hydration effect of collected powders. Hence, two peaks are located in position of 1486.95 Cm^{-1} and 1436.40 Cm^{-1}, that first peak exhibits the existence of Li_2CO_3 and the second peak represents CH_2 and CH_3 groups. All Peaks less than 1500 Cm^{-1} verify the existence of the metal-oxygen in the vibration frequencies [28]. In FTIR spectra with In-Al co-substitution, there were two weak bands in 1507Cm^{-1} and 1429Cm^{-1}, that the peaks of these regions show the asymmetric and symmetric stretching of the $–COO^-$ group. With the presence of two impurities Al and indium, the intensity of these peaks, especially below 1500 Cm^{-1}, is reduced.

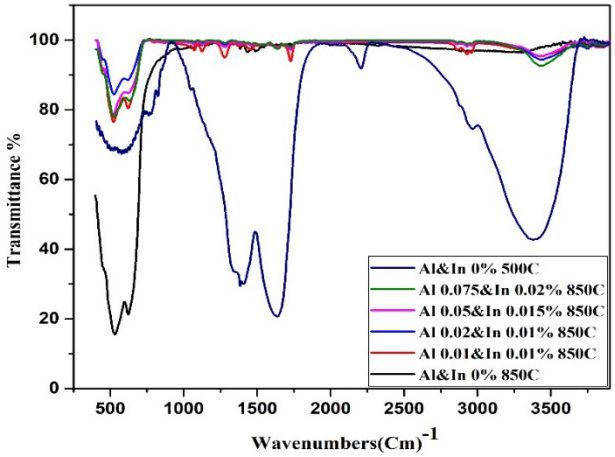

Fig. 5. FTIR spectra of the undoped $Li[Li_{0.20}Ni_{0.13}Co_{0.13}Mn_{0.54}]O_2$ and the In-Al co substitution on $Li[Li_{0.20}Ni_{0.13}Co_{0.13}Mn_{0.54}]O_2$ in temperature of 500°C and 850°C.

3.3. Electrochemical properties

Fig. 6 shows the initial charging and the discharge curves of $Li[Li_{0.20}Ni_{0.13}Co_{0.13}Mn_{0.54}]O_2$ and $Li[Li_{0.20}Ni_{0.13}Mn_{0.54-x}Co_{0.13-y}]In_xAl_yO_2$ before and after co-doped aluminum and indium impurity for different values of x and y (In&Al=0, Al&In=0.02 and 0.01%, Al&In=0.05 and 0.015%, Al&In 0.075&0.020% and Al&In=0.01 and 0.01%,) at the current density at a rate of 0.1C within V= 2–4.8 V. The diagram of the charge of all specimens is similar. During the initial charge, the charge curve for each sample is divided into two parts: 1) A growing region with a gradual increase in potential from 2 to 4.5 volts. Li^+ can be released from the main phase (eg $LiMn_{1/3}Ni_{1/3}Co_{1/3}O_2$) by the oxidation of Ni^{2+} and Co^{3+} in the form of Ni^{4+} and Co^{+4}. (2) Sloping area about 4.2 volts. During the charge, Li^+ from state of Li_2MnO_3 is oxidized to Li_2O. This results in loss of initial reversible capacity [29 and 30]. By increasing the cooping Al&In impurity with different percentages, the discharge capacity reaches to 290, 250, 204 and 230 $mAhg^{-1}$ respectively. According to the discharge capacity of the undoped sample, 255 $mAhg^{-1}$ improvement in discharge capacity in co-doping Al&In 0.02&0.01% was showed. But with the addition of impurities, was showed reduction capacity. This reduction is partly due to deprivation of oxygen for leaving of the crystalline lattice at high percentages and on the other hand, because high amounts of co-doping of aluminum and indium at the same time led to minor crystalline defects in the structure that may effect on the discharge capacity. Coulombic efficiency of samples for the percentages of Al& In= 0.02&0.01 is also highest that can be related to the more regular (well-ordered) crystal structure that simplifies the insertion/disinsertion of Li ions. The cycling efficiency for $Li[Li_{0.20}Ni_{0.13}Co_{0.13}Mn_{0.54}]O_2$ and $Li[Li_{0.20}Ni_{0.13}Mn_{0.54-x}Co_{0.13-y}]In_xAl_yO_2$ with different values of x and y (In&Al=0, Al&In=0.02&0.01%) is shown in Fig. 10 at a current density of 0.1 C in V= 2-4.8V. According to this Figure the nanopowders with co doping aluminum and indium, has showed better cyclic performance with 87% stability capacity than undoped nanopowders with 80% stability capacity due to higher surface area, and easier the insertion/disinsertion Li^+ due to larger In^{3+} ionic radius [31]. Additionally, the higher bonding energy of Al–O that is useful in preservation of the oxygen stability by stopping the oxygen release in the shape of Li_2O [32]. Nevertheless, the highest discharge capacity is acquired when the x value for the indium is 0.015, and for the aluminum, because of the highest values of the lattice parameters a and c, the y value is zero. During charge-discharge process, In^{3+} does not take part in the redox reactions. On the contrary, In^{3+} plays the role of protection column that reduces lattice contraction and ultimately leads to structure stability [33].

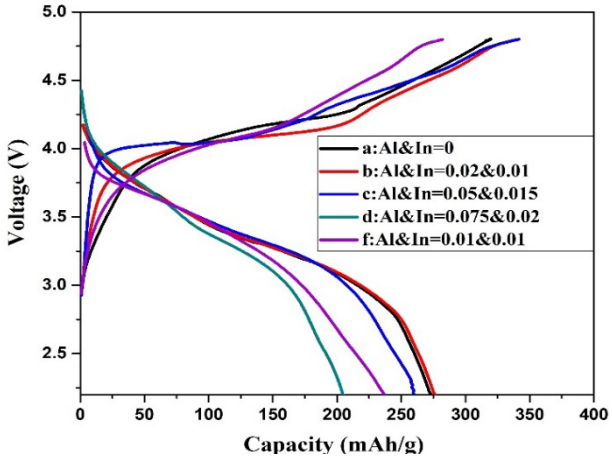

Fig. 6. The First charge–discharge curves of $Li[Li_{0.20}Ni_{0.13}Co_{0.13}Mn_{0.54}]O_2$ and the In-Al co-doping on the $Li[Li_{0.20}Ni_{0.13}Co_{0.13}Mn_{0.54}]O_2$ at different value of Aluminum and Indium.

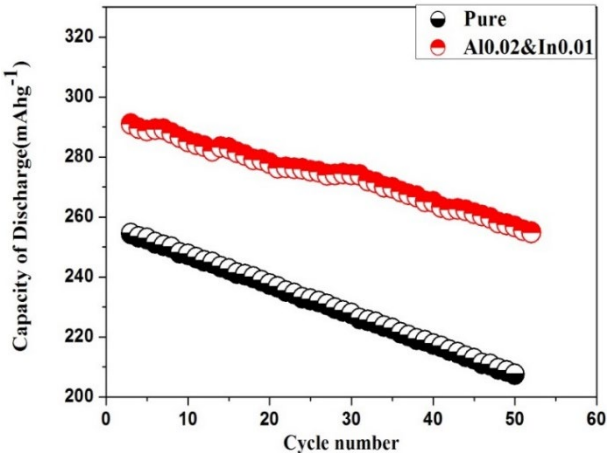

Fig. 7. The Cycling efficiency of undoped $Li[Li_{0.20}Ni_{0.13}Co_{0.13}Mn_{0.54}]O_2$ and the In-Al co-doping on the $Li[Li_{0.20}Ni_{0.13}Co_{0.13}Mn_{0.54}]O_2$ (0, Al=0.02%, In=0.01%).

The electrochemical impedance spectra (EIS) of the undoped $Li[Li_{0.20}Ni_{0.13}Co_{0.13}Mn_{0.54}]O_2$ and the In-Al co-doped on the $Li[Li_{0.20}Ni_{0.13}Co_{0.13}Mn_{0.54}]O_2$ (Al&In=0.02&0.01%) has been compared to obtain the insight for impact of the structure of the crystal on the kinetic treatment of the Li ions diffusion, and these resulting designs include the semicircle arc and a direct line, were related to process of the charge transfer and Li diffusion process in oxide structure, respectively. This analysis was performed on batteries before and after constructing cells, and also after about 50 cycles of charge and discharge. Figure 7 shows the Nyquist plots of the $Li[Li_{0.20}Ni_{0.13}Co_{0.13}Mn_{0.54}]O_2$ and the In-Al co-doped on the $Li[Li_{0.20}Ni_{0.13}Co_{0.13}Mn_{0.54}]O_2$ (Al&In=0.02&0.01%) and these diagrams include a semicircle at the high frequencies and a direct line at the low frequencies that attributed to R_{ct} charge transfer resistance and the Li diffusion process in lithium-rich layer structures [34]. After around 50 consecutive charge-discharge cycles, by comparing diameter semicircles formed R_{ct} is shown that the resistivity in the sample with co-doping Al&In 0.02&0.01% less than the undoped sample that indicates the stability of the doping sample compared to the undoped sample. Reasons for this decrease in resistance include the presence of aluminum doping that increases the electron conductivity and thermodynamic properties of the cathode [34]. Also, the presence of the doping decreases charge transfer resistance during insertion/disinsertion of Li^+ from the structure and prevents its unwanted changes and ultimately improves the electrochemical

performance. The linear relation between Z′ and $\omega^{-1/2}$ was indicated in Figures 8(b) and 8(d). Slope of the diagram σ_w corresponds to Warburg coefficient.

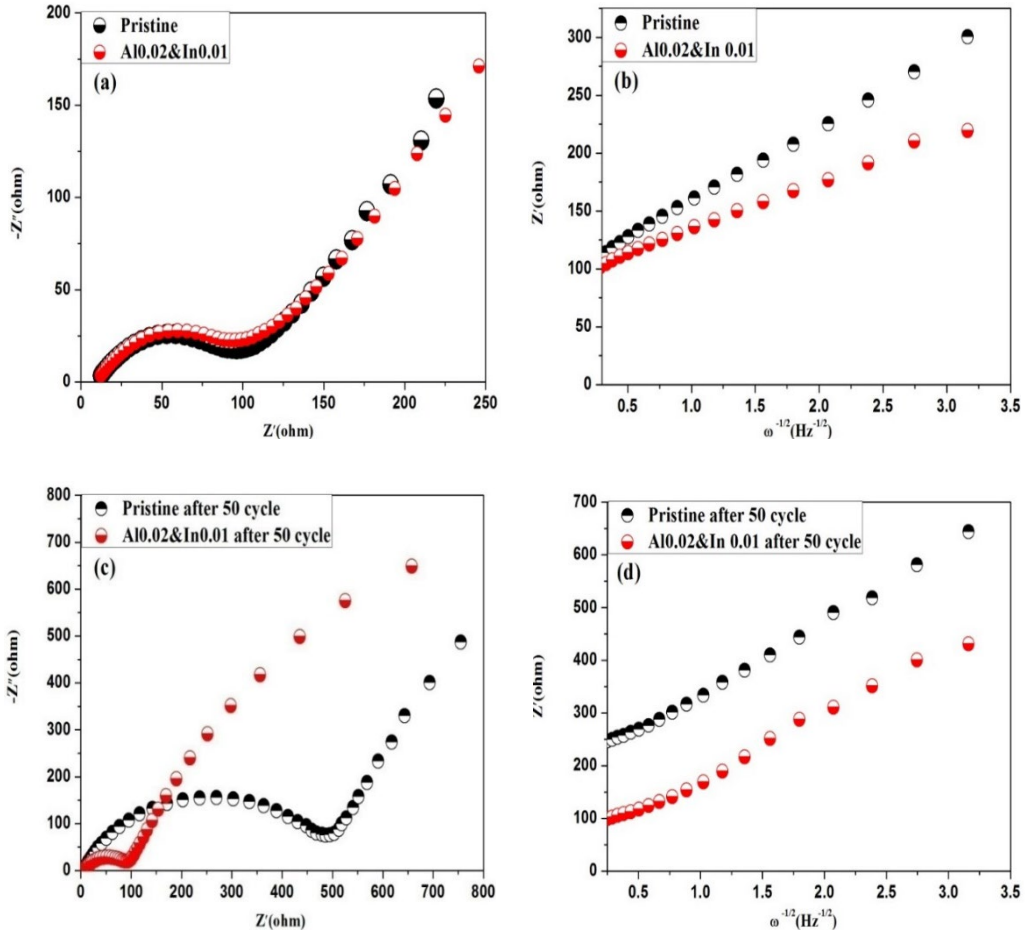

Fig. 8. (a) and (c) EIS diagram of the undoped $Li[Li_{0.20}Ni_{0.13}Co_{0.13}Mn_{0.54}]O_2$ and $Li[Li_{0.20}Ni_{0.13}Co_{0.13-0.02}Mn_{0.54-0.01}]In_{0.01}Al_{0.02}O_2$, (d) and (b) Z′ diagram according to $\omega^{-1/2}$ for before and after 50 charge-discharge cycles.

4. Conclusion

Homogeneous undoped $Li[Li_{0.20}Ni_{0.13}Co_{0.13}Mn_{0.54}]O_2$ and $Li[Li_{0.20}Ni_{0.13}Co_{0.13-y}Mn_{0.54-x}]In_xAl_yO_2$ was synthesized by the sol gel procedure. Indium-Aluminum co-doped $Li[Li_{0.20}Ni_{0.13}Co_{0.13}Mn_{0.54}]O_2$ substance showed the supreme electrochemical efficiency. Indium-Aluminum co-substitution powders shows the highest capacity maintenance when content of Aluminum and Indium is 0.02% and 0.01%, respectively. The optimal doping content of Aluminum and Indium is specified as 0.02 and 0.01. The electronic conductivity and the structural stability could be ameliorated by doping the aluminum, that this had a remarkable effect on the cycle stability; nevertheless, initial capacity is reduced. The Indium doping ameliorate the electrochemical efficiency because of an increase in the lattice parameters a and c which prepares the higher inter-slab spacing resulting in the simplification of the extraction and insertion of Li^+. According to the outcomes, Indium-Aluminum co-doping remarkably raises the electrochemical efficiency of the $Li[Li_{0.20}Ni_{0.13}Co_{0.13}Mn_{0.54}]O_2$ cathode substances in the Li-ion batteries.

References

[1] Song, MK. Park, S. Alamgir, FM. Cho, J. Liu, M. Mater Sci Eng. 72, 203-252 (2011); https://doi.org/10.1016/j.mser.2011.06.001

[2] Donghan, K. Jason, RC. Michael, MT. Electrochem Commun 36,103-106 (2013).

[3] Li, L. Song, BH. Chang, YL. Xia, H. Yang, JR. Lee, KS. Lu, L. Power Sources 283,162-170 (2015); https://doi.org/10.1016/j.jpowsour.2015.02.085

[4] Li L, Song B, Chang Y, Xia H, Yang J, Lee K, Lu L, power Sources 283, 162-170 (2015); https://doi.org/10.1016/j.jpowsour.2015.02.085

[5] Zhao J, Wang Z, Guo H, Li X, He Z, Li, Ceram Int 41, 11396-11401 (2015); https://doi.org/10.1016/j.ceramint.2015.05.102

[6] He Z, Wang Z, Cheng L, Zhu Z, Li T, Li X, Guo H, Adv Powder Technol 25, 647-653 (2014).

[7] Song B, Lai MO, Lu L, "Influence of Ru, Electrochim Acta 80 187-195 (2012).

[8] Wang D, Huang Y, Huo Z, Chen L, Electrochim Acta 107 461-466 (2013); https://doi.org/10.1016/j.electacta.2013.05.145

[9] Li Q, Li G, Fu C, Luo D, Fan J, Li L, ACS Appl Mater Interfaces, 6 10330-10341 (2014); https://doi.org/10.1021/am5017649

[10] Du J, Shan Z, Zhu K, Liu X, Tian J, Du H, J Solid State Electrochem 19, 1037-1044 (2015); https://doi.org/10.1007/s10008-014-2706-6

[11] Du K, Yang F, Hu G-r, Peng Z-d, Cao Y-b, Ryu KS, Power Sources 244, 29-34, (2013); https://doi.org/10.1016/j.jpowsour.2013.04.152

[12] Aurbach D, Srur-Lavi O, Ghanty C, Dixit M, Haik O, Talianker M, Electrochem Soc 162, 1014-1027 (2015); https://doi.org/10.1149/2.0681506jes

[13] Zhao, J. Wang, Z. Guo, H. Li, X. He, Z. Li, T. Ceram Int. 41, 11396-11401 (2015); https://doi.org/10.1016/j.ceramint.2015.05.102

[14][He, Z. Wang, Z. Cheng, L. Zhu, Z. Li, T. Li, X. Guo, H. Adv Powder Technol 25, 647-653 (2014).

[15] Song, B. Lai, MO. Lu, L. Electrochim Acta 80, 187-195 (2012); https://doi.org/10.1016/j.electacta.2012.06.118

[16] Dan, W. Yan, H. Zhenqing, H. Li, C. Electrochim Acta 107, 461-466 (2013); https://doi.org/10.1016/j.electacta.2013.05.145

[17] Li, Q. Li, G. Fu, C. Luo, D. Fan, J. Li, L. ACS Appl Mater Interfaces 6, 10330-10341 (2014); https://doi.org/10.1021/am5017649

[18] Jiangyong, D. Zhongqiang, S. Kunlei, Z. Xiaoyan, L. Jianhua, T. Haiyan, D. Solid State Electrochem 19 1037-1044 (2015).

[19] Ke, D. Fei, Y. GR, H. Peng, ZD. Cao, YB. Kwang, SR. Power Sources 244 29-34, (2013).

[20] Hao, WJ. Zhan, HH. Chen, H. Wang, YH. Tan ,QQ. Su, FB. Particuology. 33, (2013).

[21] Johnson, C. Kim, J. Lefief, C. Li, N. Vaughey, J. Thackeray, M. Electrochem Commun. 6, 1085-1091 (2004); https://doi.org/10.1016/j.elecom.2004.08.002

[22] Aurbach, D. Srur-Lavi, Ghanty, O. et al. Electrochem. Soc. 162 A1014-A1017 (2015).

[23] Ngala, J.K. Chernova, A.N. Ma, M. Mamak, M. Zavalij, P.Y. Whittingham, M.S. Mater. Chem. 14, 214-220 (2004); https://doi.org/10.1039/b309834f

[24] Na, SH. Kim, HO. Moon, CI. Mater Sci Forum. 486, 614-617 (2005); https://doi.org/10.4028/www.scientific.net/MSF.486-487.614

[25] Jiang, KC. Xin, S. Lee, JS. Kim, J. Xiao, XL. Guo, YG. Phys Chem. 14 2934-2939 (2012); https://doi.org/10.1039/c2cp23363k

[26] Wen, L. Miao, W. Xing, LG. et al. Alloys and Compounds 543, 181-188 (2012).

[27] Cheng, C X. Tan, L. Liu, H. W. and Huang, X T. Mater Res Bull. 46, 2032-2038 (2011).

[28] D. Q. Liao, C. Y. Xia, X. M. Xi, Sol-Gel Science and Technology, 78 403-408 (2016); https://doi.org/10.1007/s10971-016-3956-9

[29] G. F, Xu, J. L. Li, Q. R. Xue, Power Sources 248 894-902 (2014).
[30] Tang, T. Zhang, HL, Electrochim Acta, 191 263-269 (2016); https://doi.org/10.1016/j.electacta.2016.01.149
[31] A. Li, D. Ohsawa, Y, Power Sources, 183 344-349 (2008); https://doi.org/10.1016/j.jpowsour.2008.04.086
[32] Li X, Kehui Q, Yuyan G, Xia H, Fangdong Z, Mater Sci 50 2914-2920 (2015); https://doi.org/10.1007/s10853-015-8856-9
[33] Huang Y, Jin FM, Chen FJ, Chen L, Power Sources 256 1-7 (2014); https://doi.org/10.1016/j.jpowsour.2014.01.080
[34] Bangbang N, Jianling L, Yanying L, Zhanyu L, Zhe Y. Ceramics International 45 12484-12494 (2019).